Origin of Ultralow Thermal Conductivity in Metal Halide Perovskites

Sandip Thakur and Ashutosh Giri*

Department of Mechanical, Industrial and Systems Engineering, University of Rhode Island, Kingston, RI 02881, USA

E-mail: ashgiri@uri.edu

Abstract

Resulting from their remarkable structure-property relationships, metal halide perovskites have garnered tremendous attention in recent years for a plethora of applications. For instance, their ultralow thermal conductivities make them promising candidates for thermoelectric and thermal barrier coating applications. It is widely accepted that the 'guest' cations inside the metal halide framework act as 'rattlers', which gives rise to strong intrinsic phonon resistances, thus explaining the structure-property relationship dictating their ultralow thermal conductivities. In contrast, through systematic atomistic simulations, we show that this conventionally accepted 'rattling' behavior is not the mechanism dictating the ultralow thermal conductivities in metal halide perovskites. Instead, we show that the ultralow thermal conductivities in these materials mainly originate from the strongly anharmonic and mechanically soft metal halide framework. By comparing the thermal transport properties of the prototypical fully-inorganic $CsPbI_3$ and an empty PbI_6 framework, we show that the addition of Cs^+ ions inside the nanocages leads to an enhancement in thermal conductivity through vibrational hardening of the framework. Our extensive spectral energy density calculations show that the Cs^+ ions have well-defined phase relations with the lattice dynamics of the 'host' framework resulting in additional pathways for heat conduction, which is in disagreement with the description of

the individual 'rattling' of guests inside the framework that has been widely assumed to dictate their ultralow thermal conductivities. Furthermore, we show that an efficient strategy to control the heat transfer efficacy in these materials is through the manipulation of the framework anharmonicity achieved via strain and octahedral tilting. Our work provides the fundamental insights into the lattice dynamics that dictate heat transfer in these novel materials, which will ultimately help guide their further advancement in the next-generation of electronics such as in thermoelectric and photovoltaic applications.

Keywords

Lead halid perovskites, thermal conductivity, phonon transport, octahedral tilting, anharmonicity

I. Introduction

Owing to their remarkable physical properties such as enhanced carrier lifetimes,[1–4] facile processability,[5–9] high absorption coefficients,[10] and ultralow thermal conductivities,[11–13] metal halide perovskites are currently one of the most intriguing and widely studied materials. Their physical attributes position them as prime candidates for use in applications such as the next generation of photovoltaics,[14–16] light-emitting diodes,[17–19] lasers,[20,21] optoelectronics,[22,23] and thermoelectrics.[24]

The remarkable physical properties of metal halide perovskites mostly arise from their ABX_3-type crystalline structure where the corner-sharing BX_3^- octahedra with metals (e.g., Pb^{2+}, Sn^{2+}) at the center and halide anions (e.g., Cl^-, Br^-, I^-) at the corners form a network of three-dimensional anion cage capable of hosting A-site cations (e.g., Cs^+ or an organic cations such as methylammonium, MA^+). Most notably, accompanying the soft and highly flexible framework[25] of metal halide perovskites is the coexistense of a variety of highly anharmonic motions of the different ions,[26] that are shown to be responsible for not only their unrivaled optoelectronic properties,[27–29] but also for their unique vibrational physics dictating their ultralow thermal conductivities.[12,25,30–33]

However, a complete understanding of the influence of the intrinsic anharmonicity, especially in terms of the dynamic motion of the A-site cation, on the ultralow thermal conductivities in perovskites is still lacking. This lack of understanding limits our ability to properly engineer their thermal transport properties, which is one of the main factors underpinning their applicability for the aforementioned applications.

In general, dating back to the early work by Peierls in 1929,[34] the description of heat conduction in most nonmetallic crystals (and the lattice contribution of metals) have been rooted in the widely accepted phonon gas models (PGM).[35,36] In the PGM, heat is primarily carried by propagating wave packets with well-defined group velocities (forming the diagonal elements of the phonon velocity operator),[37] thus resembling gas particles moving and scattering with each other to conduct heat. Although this model has been extensively used over the past several decades to describe and predict heat conduction in many classes of solids,[38–44] for disordered systems and complex crystals with large unit cells, theories reliant on the PGM fail to capture the intrinsic mechanisms responsible for the overall heat transfer.[45–48] This has mainly been ascribed to the fact that the heat carrying vibrations in these systems lack plane wave characteristics and do not possess well-defined group velocities that are pre-requisites for correctly predicting vibrational heat transfer via the PGM. In such scenarios, where Peierls' PGM breaks down, a different theory pioneered by Allen and Feldman has been successful in describing the glass-like thermal conductivities.[45,49] Their description of heat conduction (in contrast to the PGM) is rooted in the harmonic theory for glasses where vibrational modes couple and transfer their energies (differently than plane waves) through the off-diagonal elements of the velocity operator. Subsequently, recent theoretical advancements have extended this harmonic formulation by Allen and Feldman to anharmonic systems where the phonon linewidths are larger than the inter-branch spacings;[47,48] for some complex crystals with large unit cells, the phonon branches are closely bunched together and the strong anharmonicity leads to large broadening of the branches that ultimately result in ultralow or glass-like thermal conductivities for those crystalline solids.

In metal halide perovskites, thermal transport has been shown to be at an intersection of the

crystal-like and the glass-like regimes, where the disorder from the soft BX_3 framework along with the coupling of the vibrational modes of the framework with the resonant vibrations of the guest A-site cations renders the conventional PGM insufficient in describing the heat conduction.[32,50–52] Rather, the description of transport has been explained through a mixed phononic and non-phononic characteristics, with the low-frequency acoustic modes (that are dictated by the inorganic framework) retaining features of phononic transport, while the higher frequency optical modes contribute via the off-diagonal components of the velocity vector to the overall thermal conductivity.[32,47,52] In fact, utilizing a unified theory of thermal conductivity for solids that takes into account both the phononic and non-phononic characteristics, Simoncelli *et al.*[47] have shown that the majority of the contribution ($\sim 70\%$) to the overall thermal conductivity in $CsPbBr_3$ comes from these non-phononic vibrations at room temperature. Moreover, their ultralow thermal conductivities are thought to mainly arise from strong anharmonicity induced from the localized modes originating from the 'rattling' motion of the Cs^+ ions inside the perovskite cages.[33,52]

The 'rattling' picture has been widely accepted to be the main factor suppressing the lattice thermal conductivity in many framework structures where these localized anharmonic vibrations scatter the long wavelength acoustic phonons in clathrates,[53–56] skutterudites,[57–59] and other complex unit cell compounds.[60,61] This 'rattling' behavior is mainly prescribed to the weakly bound dynamics of the cations occupying the nanocages. In this regard, for metal halide perovskites, first-principles calculations have shown that the band crossings (and hybridizations) between acoustic modes dictated by the BX_3 framework and optical modes originating from the Cs rattling motion lead to the unprecedented anharmonicity and ultralow thermal conductivities in these materials.[33,52,62] Recently, several works have been carried out to study the interactions between the A-site cations and the inorganic framework and their effect on the overall heat transfer across metal halide pervoskites.[63–68] For instance, Hata *et al.* employed *ab initio*-based MD simulations on $MAPbI_3$ and showed that the coupled translational and rotational motions of MA^+ cations interact with and scatter the heat carrying acoustic phonons and low-lying optical modes associated with the Pb-I framework resulting in their reduced thermal conductivity.[63] Similarly, Yue *et al.*'s fully first-

principles calculations on $MAPbI_3$ demonstrated that the collective motions of the organic cluster interacting with the inorganic cage drags thermal transport in these materials.[65] Experimentally, by measuring the thermal conductivities of $MAPbI_3$ and $MAPbBr_3$ nanowires, Wang *et al.*[68] have shown that the larger lattice spacing with the smaller bromide atoms leads to more dynamic disorder of the MA^+ cations and lower resulting thermal conductivities in $MAPbBr_3$. They also show that the thermal conductivity in $CH_3NH_3PbX_3$ nanowires (X= I, Br) is significantly reduced due to cation dynamic disorder as compared to that of $CsPbBr_3$ nanowires. Likewise, Elbaz *et al.*[13] employed frequency-domain thermoreflectance measurements to report varying thermal conductivities in the range of 0.34 to 0.73 W m^{-1} K^{-1} for various metal halide perovskites including $MAPbX_3$ (X= Cl, Br, I), $CsPbBr_3$, and $FAPbBr_3$. All of these aforementioned works highlight the strongly anharmonic nature of the metal halide frameworks and the dynamic disorder of the cations inside the cages that ultimately reduce the overall thermal transport in these materials.

While it is intuitive to consider the reduction in thermal conductivity due to the dynamic disorder introduced from the rattling motion of the Cs atoms inside the relatively oversized cages, it could also be expected that filling of the void spaces in the highly anharmonic and soft metal halide frameworks could also potentially lead to an increase in the efficacy of the heat transfer; in solids, increase in atomic density is typically associated with higher thermal conductivities,[69,70] which suggests that filling the nanopores in BX_3 framework should result in an overall increase in thermal conductivity. Moreover, the insights gained from first-principles calculations on metal halide perovskites that only consider three-phonon interactions[33,47,52] might not be sufficient to capture all the higher-order vibrational interactions that dictate the anharmonicity (and ultimately the thermal properties) in these systems. In this regard, molecular dynamics (MD) simulations offer the prospect of capturing the true anharmonicity through intrinsically incorporating all the higher order interactions (that include the interactions between the A-site cations and the soft octahedral framework), thus allowing for the complete description of their vibrational physics.

Here, by conducting systematic MD simulations on $CsPbI_3$, the prototypical fully-inorganic metal halide perovskite, we comprehensively show that the reduced thermal conductivity in these

perovskites is not the consequence of the rattling of Cs^+ ions inside the nanocages, but is the result of the intrinsically and strongly anharmonic nature of the PbI_6 octahedral framework. Specifically, by comparing the thermal properties of empty (without the A-site cation, Cs^+ ions) and filled $CsPbI_3$ structures, we show that the Cs^+ ions indirectly facilitate heat transfer by hardening the vibrational modes of the soft octahedral framework, a result which is counterintuitive to the 'rattling' picture associated with lowering the thermal conductivity of similar framework materials.[53–61] From our extensive spectral energy density (SED) calculations, we also reveal that (on average) the anharmonicity is increased and the individual phonon lifetimes are reduced by filling the nanocages which in the PGM, typically leads to the reduction in the thermal conductivity. In contrast, from our Green-Kubo (GK) calculations of thermal conductivity under the equilibrium MD framework that fully accounts for the intrinsic anharmonicities of the systems, we find that the thermal conductivity of the empty perovskite is reduced in comparison to the filled $CsPbI_3$ structure. We unequivocally show that the additional channels due to the vibrational hardening of the framework leads to the overall increase in the thermal conductivity of the $CsPbI_3$ structure as compared to the empty PbI_6 framework, which is in direct contrast to the conventionally accepted picture of 'rattling' where the dynamics of the A-site cations are ascribed to dominate the phonon scattering mechanisms leading to their ultralow thermal conductivities. Finally, we show that a strategy to further lower the thermal conductivity in these highly anharmonic perovskites is through increasing the octahedral tilting that results in increased disorder of the framework, which is key to controlling the heat conduction mechanisms in metal halide perovskites.

II. Results and Discussions

Figure 1 shows the temperature dependent thermal conductivities for our $CsPbI_3$ and an empty PbI_6 framework structures. For our $CsPbI_3$ structure (γ-orthorhombic phase), the room temperature thermal conductivity of 0.56 ± 0.06 W m^{-1} K^{-1} agrees very well with the experimentally determined value of 0.45 ± 0.05 W m^{-1} K^{-1} for $CsPbI_3$ nanowires (δ-orthorhombic phase).[12] We

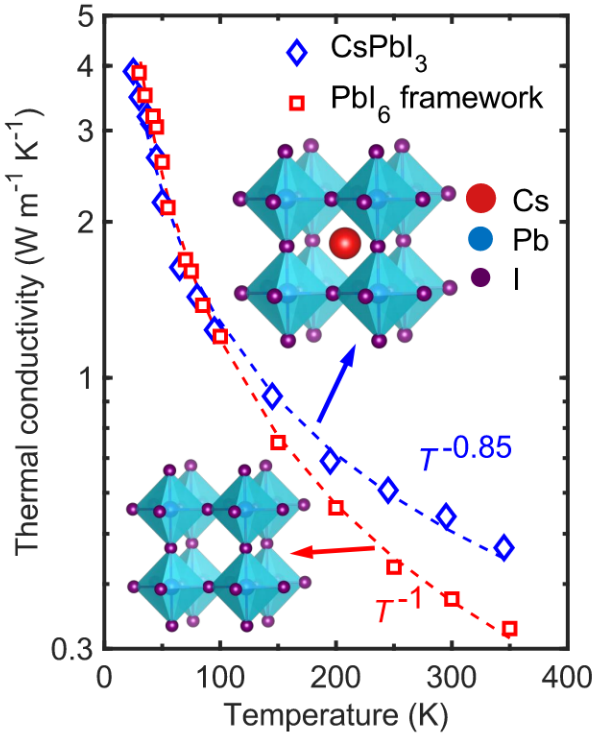

Figure 1: Calculated thermal conductivities as a function of temperature for $CsPbI_3$ compared to an empty PbI_6 framework structure without the Cs^+ ions occupying the void spaces between the octahedras. For both structures, the thermal conductivity follows a temperature dependence akin to crystalline solids, which has been attributed to anharmonic phonon-phonon scattering. The slightly weaker temperature dependence for the $CsPbI_3$ (with $\sim T^{-0.85}$ trend) suggests that along with anharmonic scattering, disorder scattering due to the Cs^+ ions also plays a role as compared to the empty case where it follows the typical T^{-1} trend. The higher thermal conductivities at higher temperatures for $CsPbI_3$ as compared to the empty framework suggests that the inclusion of Cs^+ ions inside the octahedral cages leads to additional channels of heat transfer.

note that the uncertainties in our reported thermal conductivities are determined from five independent simulations and are in the range of 10-12% for all reported thermal conductivities throughout this work. The slight discrepancies between the experiments[12] and our MD results might arise due to variation in $CsPbI_3$ phase along with the classical nature of MD simulations where all the vibrational modes are activated at all temperatures and fails to replicate the quantum effects prevalent in experimental measurements at temperatures below the Debye temperature of the material. For both structures, the thermal conductivities show a crystalline-like behaviour where the thermal conductivity decreases with increasing temperature, which is attributed to anharmonic phonon-phonon scattering mechanisms (or Umklapp scattering processes). In comparison to the empty PbI_6 struc-

ture, our $CsPbI_3$ shows a comparatively reduced temperature dependence. This deviation from the typical $1/T$ dependence is indicative of disorder scattering introduced by filling the nanocages with the guest Cs^+ ions.[38,40,43] More interestingly, although the thermal conductivities of the filled and empty structures are similar for lower temperatures below 100 K, at higher temperatures the thermal conductivity of the filled structure is higher (by a factor of $\sim$1.5 at room temperature). This is surprising since it is widely believed that in such framework systems, the rattling of the 'guest' ions (Cs^+ in this case), is expected to lower the thermal conductivity.[12,33,52] As such, filling the nanocages with the Cs^+ ions should have lowered the thermal conductivity throughout the entire temperature range if the rattling scenario was the dominant scattering mechanism. Instead, the relatively higher thermal conductivities of the filled structure suggest that additional channels of heat transfer are introduced by filling the voids with the Cs^+ ions. We note that the crystalline structure of the PbI_6 framework remains intact and there are no considerable changes in the radial distribution function of the atoms with the removal of the Cs^+ ions (Fig. S6).

To understand the intrinsic role of Cs^+ ions in dictating the temperature-dependent thermal conductivity of $CsPbI_3$, we compare the vibrational density of states (DOS) of the PbI_6 framework in the filled and empty structures as shown in Fig. 2a. For both temperatures, 50 K (Fig. 2a) and 300 K (Fig. S8), considerable vibrational hardening is observed for the filled structure as compared to the empty framework. Moreover, additional vibrational modes (near $\sim$2 THz frequency as highlighted by the arrow in Fig. 2a) appear more pronounced in the vibrational spectrum of the PbI_6 framework in the filled structure as compared to the empty structure. These additional modes in the filled structure are responsible for carrying a substantial amount of heat (see Fig. S9) and ultimately leads to the higher thermal conductivities for the filled case as compared to the empty structure at higher temperatures (see Fig. 1). In fact, our spectrally decomposed heat flux calculations show that frequencies $>$1.5 THz (that are predominantly optical phonons) contribute $\sim$70% of the total room temperature thermal conductivity in both structures as shown in Fig. S9. Similar observations of high contributions from optic modes have been reported for Cs_2SnI_6,[52] $CsPbBr_3$,[47] and other low thermal conductivity solids.[71,72] The additional modes arise due to the increase in the stiffness

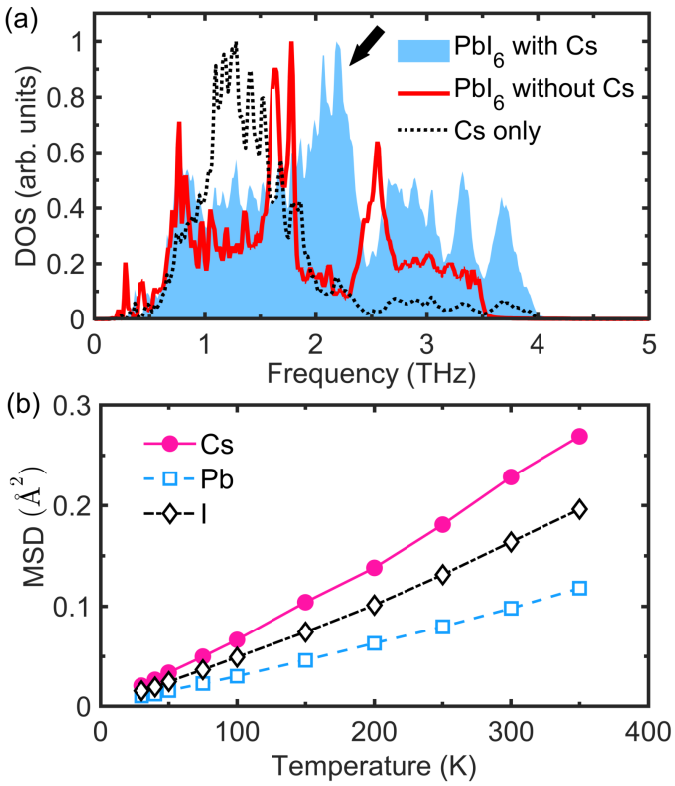

Figure 2: (a) Vibrational density of states of the PbI_6 framework for $CsPbI_3$ with and without the Cs^+ ions occupying the nanocages at 50 K. For comparison, the DOS of the Cs^+ ions for $CsPbI_3$ are also shown. Considerable phonon hardening occurs with the inclusion of the Cs^+ ions. The density of vibrational modes $\sim$ 2 THz also increase with the addition of the Cs^+ ions. (b) Calculated mean square displacements as a function of temperature for the different atomic species in $CsPbI_3$. At low temperatures, the MSDs of the atoms are similar. At higher temperatures, the MSD of Cs^+ ions increase more rapidly, signifying that these ions experience larger thermal displacements.

that is observed when the cages are filled with the Cs cations (see Fig. S13).

Figure 2b shows the mean square displacement (MSD) of the various atomic species as a function of temperature for our $CsPbI_3$ domain. At low temperatures (<100 K), the MSD for all three atomic species are similar, but with increasing temperature, the MSD of the Cs^+ ions increase more rapidly. This highlights the potential role of Cs^+ ions in dictating the difference in the temperature dependent thermal conductivity behavior for the filled and empty structures where the thermal conductivities are similar at lower temperatures and deviates at higher temperatures where the dynamic motion of the Cs^+ ions are more pronounced. Typically, this pronounced motion of the guest atoms have routinely been associated with anharmonic rattling modes responsible for the

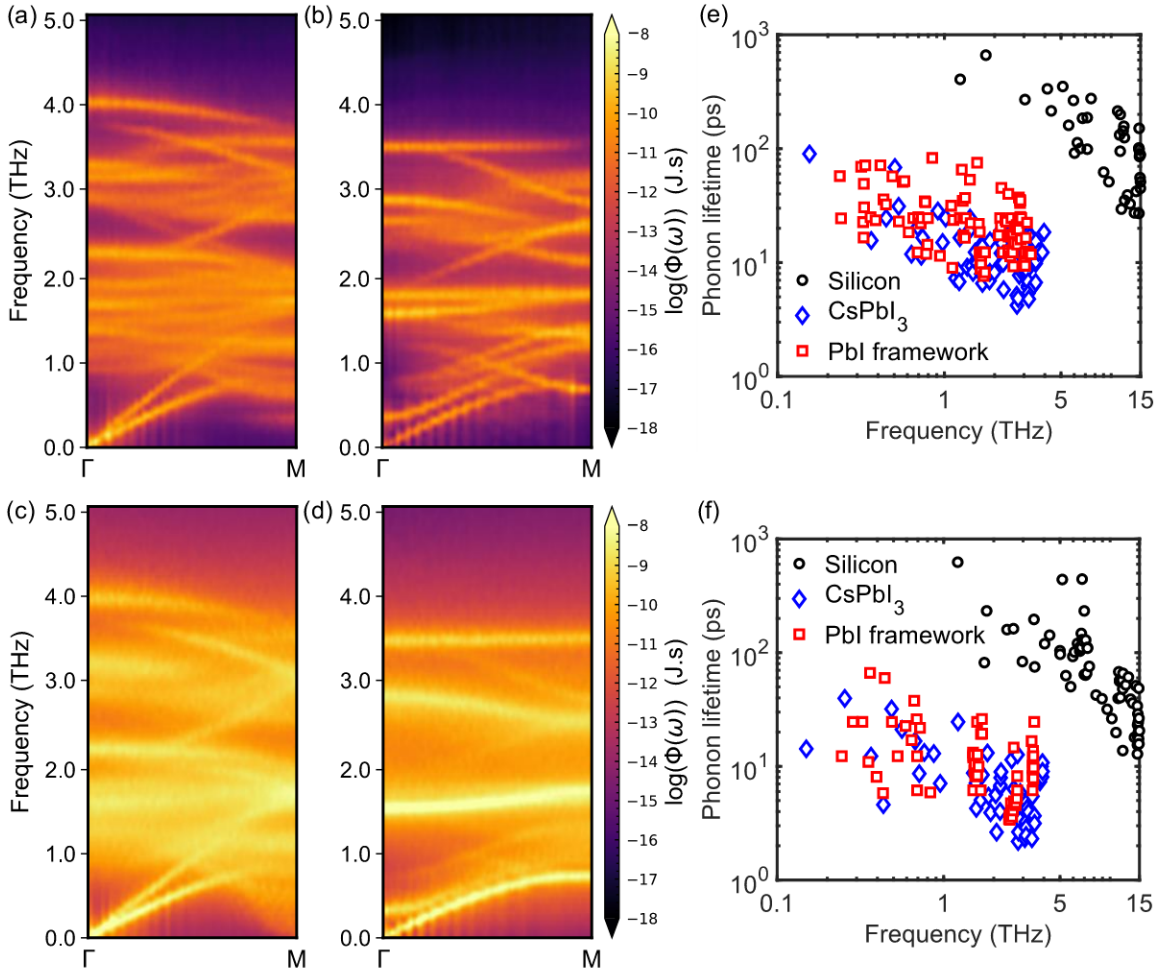

Figure 3: Calculated phonon spectral energy densities for (a) $CsPbI_3$ (b) empty PbI_6 framework at 50 K. Calculated phonon spectral energy densities for (c) $CsPbI_3$ (d) empty PbI_6 framework at 300 K. The shading indicates the magnitude of the spectral energy density. The number of optic modes in the 1-3 THz range is significantly reduced with the removal of the Cs^+ ions from the nanocages, which also results in phonon softening. Considerable broadening in the spectral energy density at the higher temperature signifies reduced phonon lifetimes of the vibrational modes as shown in (e) at 50 K and (f) 300 K. In comparison to the phonon lifetimes in a typical semiconductor such as silicon (filled circles), the phonon lifetimes in $CsPbI_3$ is more than an order of magnitude lower, which highlights their strongly anharmonic nature. On average, the phonon lifetimes in the $CsPbI_3$ structure is lower than in the empty PbI_6 framework.

strong intrinsic phonon resistance and suppression of thermal conductivity in skutterudites,[57–59] clathrates,[53–56] and half-Heuslers.[73,74] While this may, in part, present phonon resistive processes due to avoided crossings in the acoustic phonon modes, the role of the guest atoms in metal halide perovskites is more complicated than just the 'rattling' picture in terms of dictating their thermal

transport mechanisms. More specifically, these guest atoms are responsible for additional modes that facilitate heat transfer indirectly through the host framework as shown by our extensive analyses discussed below.

To gain further insights into the role of Cs^+ ions in dictating the thermal conductivity of $CsPbI_3$, we perform phonon SED calculations for both the filled and empty structures;[75,76] further details of the calculations are given in the Methods section. Figures 3a-d show the comparison of SED for our filled and empty structures at low (50 K) and high (300 K) temperatures. For both temperatures, we find that the structures possess considerable anharmonicity as compared to a typical crystalline solid such as silicon (Fig. S12). This is represented by the higher contrast in the shading of the plot, which relates to the higher magnitude of SEDs and is indicative of higher kinetic energies of the vibrational modes. As such, the higher SEDs along with the increase in their broadening shows that, on average, the vibrational modes in both our filled and empty structures experience considerable anharmonicity and vibrational scattering with shorter vibrational lifetimes as compared to typical crystalline semiconductors such as silicon. This is exemplified in Figs. 3e and 3f, where we show the phonon lifetimes as predicted from our SED calculations for our structures as compared to that of silicon at 50 K and 300 K, respectively. For both temperatures, the phonon lifetimes of the specific modes in silicon are at least an order of magnitude higher than the corresponding lifetimes for the modes in both the filled and empty structures. More interestingly, although less pronounced at the lower temperature, our SED and phonon lifetime calculations show that removing the Cs^+ ions from the framework does not lead to a lesser broadening of the phonon modes as might be expected in the case of the 'rattling' behavior. In contrast, the addition of Cs^+ ions inside the nanocages leads to a better definition of the the wave-vectors for the longitudinal mode, which appear to be considerably broadened for the empty case. Furthermore, even for the empty structure, we observe low lying optic modes forming avoided crossings with the acoustic mode, thus further emphasizing the intrinsic anharmonicity of the PbI_6 framework. However, consistent with our DOS calculations, there are also higher densities of optical modes present in the 1-3 THz range in the filled structure with similar phonon lifetimes albeit with larger dispersions of the optic

modes as compared to that in the empty PbI_6 framework. These additional optic modes carry a significant amount of heat at room temperature in the filled $CsPbI_3$ structure as shown in Fig. S9 of the Supporting Information from our spectrally decomposed heat flux calculations. This helps explain the higher thermal conductivities of the filled structure at relatively higher temperatures as shown in Fig. 1. Recently, a unified transport theory of thermal conductivity in solids has identified wave-like tunneling between the tightly packed and anharmonic optical branches to considerably dictate thermal conductivity at higher temperatures in these types of metal halide perovskite structures.[47] Considering this, the additional optical branches that are introduced by filling Cs^+ ions inside the cages (see Fig. 3) should result in greater heat conduction at higher temperatures from these modes through wave-like tunneling across the tightly packed (and strongly anharmonic) optical branches. Taken together, our comparison of the SED calculations for the empty and filled structures reveal that the anharmonicity in these materials is strongly driven by the PbI_6 framework and the addition of the Cs^+ ions leads to more optic modes that could facilitate heat transfer in these materials.

In the context of the PGM, the reduced phonon lifetimes of the filled structure when compared to the empty case (Figs. 3e and 3f) would result in lower thermal conductivities for the filled case for both high and low temperatures. However, our GK calculations show that the thermal conductivity is similar at lower temperatures and, in contrast to the typical behavior of crystalline solids well described by the PGM, the thermal conductivity is higher for the filled case at higher temperatures even though the average phonon lifetimes are lower. Therefore, only considering the phonon lifetimes does not provide a comprehensive understanding of the vibrational physics in these highly anharmonic materials where the non-phononic characteristics largely dictates the heat conduction.

In the 'rattling' description of thermal transport, it is expected that the decoupled dynamics of the 'guest' atoms serves as resistive decay channels for heat carrying acoustic modes of the 'host' framework.[77] However, separating the SED contributions of the Cs^+ ions from that of the PbI_6 framework (as shown in Fig. 4), we find that the Cs^+ ions are associated with the soft acoustic branches corresponding to the very low transverse ($v_{TA,g}$ = $\sim$1054 m s^{-1}) and longitudinal ($v_{LA,g}$

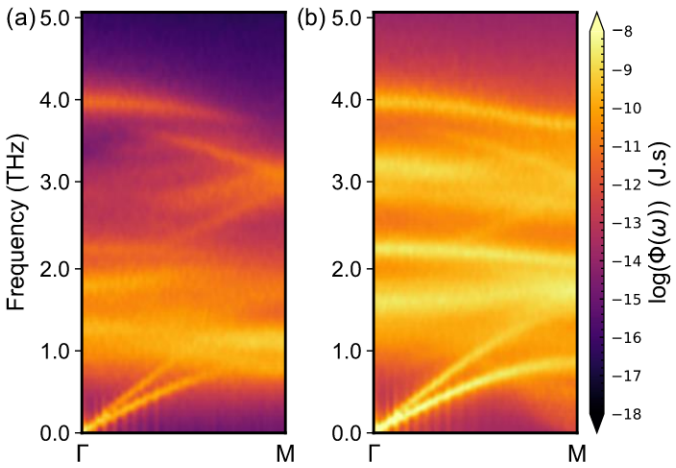

Figure 4: Calculated phonon spectral energy densities for (a) Cs^+ ions and (b) PbI_6 framework for our $CsPbI_3$ structure. The Cs^+ ions are associated with the soft acoustic branches. Along with the addition of higher densities of vibrations in the 1-2 THz range, the Cs^+ ions also show well-defined phase relations with the PbI_6 framework throughout the entire vibrational spectrum.

= ∼2046 m s^{-1}) group velocities. Note, these sound speeds determined from our MD simulations match very well with experimentally determined values for lead halide perovskites.[13] We also find that there is well-defined phase relations between the framework and the A-site cations as shown by the SED calculations in Fig. 4 throughout the entire vibrational spectrum. This again supports the notion that the picture of freely 'rattling' A-site cations inside the metal halide framework (as has been conventionally accepted to lower thermal conductivity) is not the dominant mechanism dictating heat transfer in these perovskites. To support this further, we fictitiously change the mass of Cs^+ ions (from 32 to 400 g mol^{-1}) to vary the spectral overlap with the PbI_6 framework. As shown in Fig. S11, changing the mass has negligible influence on the temperature dependent thermal conductivity. This suggests that Cs^+ ions are indirectly affecting thermal transport since it is the phonon hardening resulting from the interaction of the Cs^+ ions with the PbI_6 framework that leads to the additional channels of heat transfer in these materials.

To dig deeper into the role of the dynamic motion of the Cs^+ ions in dictating the vibrational characteristics of $CsPbI_3$, we also perform additional simulations where we freeze the different degrees of freedom of Cs^+ ions in $CsPbI_3$ structure and compare the temperature dependent thermal conductivity to the original $CsPbI_3$ domain considering all of the degrees of freedom as shown in

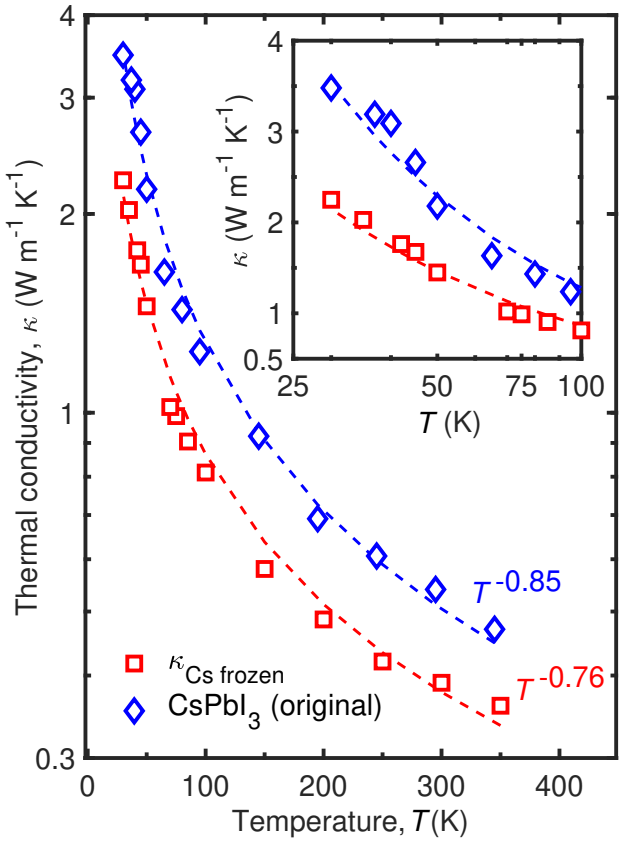

Figure 5: Thermal conductivity as a function of temperature for $CsPbI_3$ structure and a constrained $CsPbI_3$ domain where we restrict the degrees of freedom for the Cs^+ ions (which are essentially frozen inside the nanocages). The constrained domain has a lower thermal conductivity for the entire temperature range, highlighting the role of Cs^+ ions in providing additional channels of heat transfer.

Fig. 5. The thermal conductivity of the constrained domain is lower than the original structure throughout the temperature range with a reduced $T^{-0.76}$ trend. This reduction in thermal conductivity further supports our observation that the dynamic motion of the Cs^+ ions facilitates heat transfer. Further SED calculations of the constrained domain as shown in Fig. S13 of the Supporting Information emphasizes the role of Cs^+ ions in dictating the soft acoustic modes in $CsPbI_3$, where these modes vanish for the constrained domain. Moreover, the thermal conductivity of the constrained domain without the soft acoustic modes is reduced by $\sim$30-40% across the entire temperature range in comparison to the thermal conductivity of the original structure. This alludes to the reduced contributions from the acoustic modes (with propagating nature) in $CsPbI_3$ since even

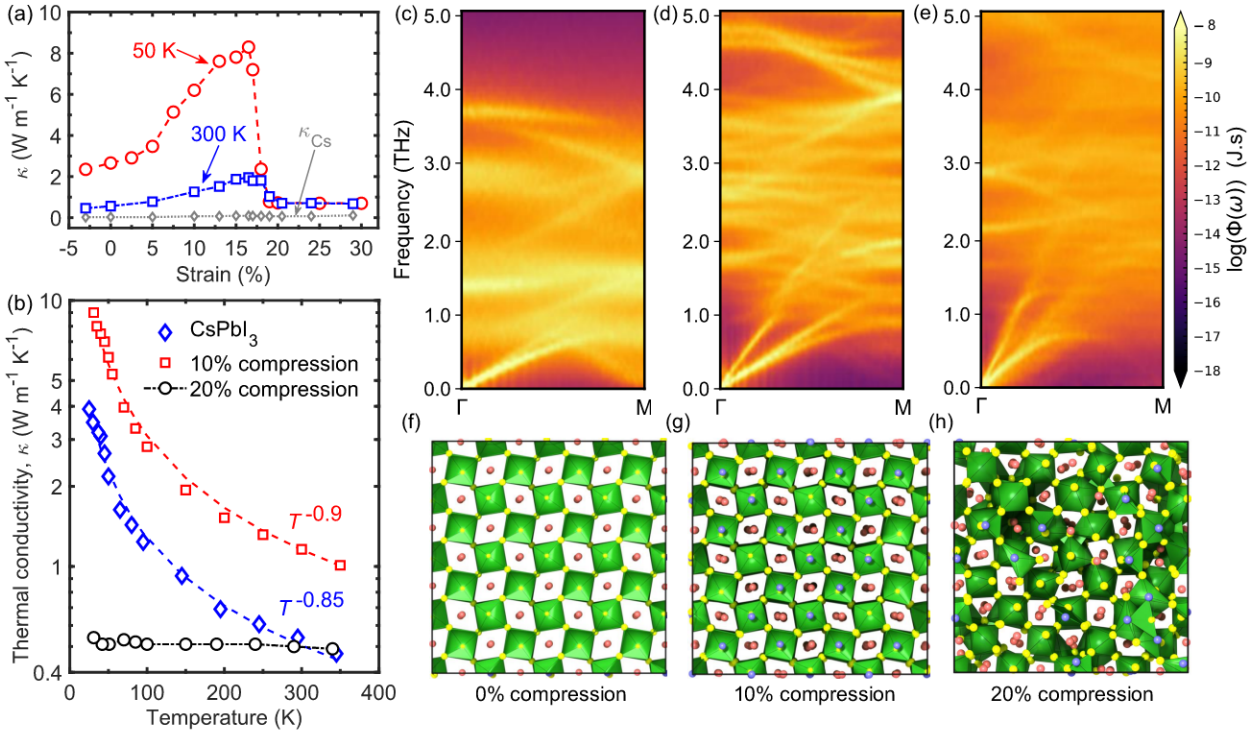

Figure 6: (a) Thermal conductivity as a function of hydrostatic strain at 50 K and 300 K temperature. For hydrostatic strain levels up to ∼18%, the thermal conductivity increases monotonically for both temperatures as a result of phonon hardening and increase in the group velocities of phonons. For higher strain levels, the thermal conductivity abruptly decreases, which we ascribe to disorder induced vibrational scattering from increased octahedral tilts. (b) Comparison of thermal conductivities as a function of temperature for our $CsPbI_3$ structures at 0%, 10%, and 20% hydrostatic compressions. The structure with 10% compression shows a similar crystalline-like temperature trend, whereas increasing the hydrostatic compression to 20% leads a temperature independent thermal conductivity, which is indicative of disorder scattering dominated heat transfer. Calculated phonon spectral energy densities of $CsPbI_3$ structure at 300 K for (c) 3% hydrostatic tensile strain (d) 10% percent and (e) 20% hydrostatic compressions. Considerable phonon hardening and group velocity increase leads to enhancement in thermal conductivity of the $CsPbI_3$ structure under 10% hydrostatic compression. Although further increase in hydrostatic strain levels of up to 20% leads to increase in group velocities for the acoustic modes near the Brillouin zone center, the group velocities for acoustic phonon modes away from the zone center is considerably reduced. This is attributed to enhanced disorder from increased octahedral tilting. Top view showing the PbI_6 framework tilt for (f) 0% percent (g) 10% percent and (h) 20% percent hydrostatic compressions.

without these modes (as in the case of our constrained structure), the thermal conductivity is only 30-40% lower than our original $CsPbI_3$ structure. This supports our spectrally decomposed heat flux calculations (Fig. S9) where we have shown the dominant role played by the higher frequency

optic modes (>1.5 THz). Moreover, this is in line with recent findings from Simoncelli *et al.*,[47] for $CsPbBr_3$ crystals where they calculate $\sim$30% contribution from phonon-like propagating modes through the calculations from their unified theory.

Finally, to understand the driving mechanism behind the ultralow thermal conductivities in these perovskites, we perform GK calculations on $CsPbI_3$ structures with varying levels of hydrostatic strain in order to influence their anharmonic and mechanically soft nature. Note, the interatomic potential utilized in this work has been specifically developed to correctly reproduce the total energy of the lead halide perovskites under hydrostatic deformations along with correctly replicating the energy profiles of the A-site cations that reorient with respect to the deforming framework.[78] As shown in Fig. 6a for both the high and low temperatures, we find that the thermal conductivity increases as a function of hydrostatic compressive strains up to $\sim$18%. For higher strain levels, however, the thermal conductivity decreases sharply to a value of $\sim$0.5 W m^{-1} K^{-1} for both temperatures. It is also interesting to note that there is negligible contribution directly from the Cs^+ ions towards the total thermal conductivity, which is mainly dictated by the PbI_6 framework. The increasing trend in thermal conductivity with the application of compressive strain can be attributed to the vibrational hardening of the PbI_6 framework. This is evident from the MSDs of the atoms where the MSD of both the PbI_6 framework and Cs^+ ions decreases considerably throughout the temperature range (see Fig. S10). However, there is negligible contribution from Cs^+ ions (Fig. 6a) in the overall thermal conductivity for all strain levels, showing that the PbI_6 framework dictates thermal transport. Further temperature-dependent calculations for domains under the 10% and 20% strain levels (Fig. 6b) show that while the crytalline-like temperature trend holds for 10% strain, the temperature trend (or the lack thereof) for the highly strained case demonstrates a completely different mechanism (namely disorder scattering) that dictates the thermal conductivity for $CsPbI_3$ domains at higher strain levels. Furthermore, the vibrational spectrum are shifted to higher frequencies with increasing strain levels as shown by our SED calculations in Fig. 6c-e. We also observe increasing group velocities of the acoustic branches as indicated by the larger slopes of the acoustic branches with increasing hydrostatic strain. However, with

compressions beyond $\sim 18\%$, although the group velocities near the Brillouin zone center are increased, there is considerable hybridization of the acoustic phonons and the optic modes away from the Brillouin zone center. Along with considerable broadening of the vibrational modes throughout the entire spectrum as shown in Fig. 6e, hydrostatic compressions beyond $\sim 18\%$ lead to an overall reduction in the heat transport. Comparing the octahedral tilts for structures beyond this strain level with the tilts for the lower strains (see Fig. 6f-h), it is evident that the pronounced tilts lead to considerable disorder scattering, which counteracts any increments in heat conduction due to phonon hardening with higher strains. These results further emphasize the significant role of the PbI_6 octahedral framework in dictating the thermal conductivity of these inorganic halide perovskites. Considering this, a strategy to manipulate heat conduction in these materials could be to alter the PbI_6 octahedral framework tilts that dictate thermal transport properties in these soft and intrinsically anharmonic materials.

III. Conclusion

To summarize our findings on the origin of the ultralow thermal conductivities in metal halide perovskites: (i) the considerable anharmonicity associated with the phonon modes in the entire vibrational spectrum of $CsPbI_3$ results in reduced lifetimes and low group velocities in these materials. (ii) In contrast to the conventionally accepted notion of 'rattling' leading to higher phonon resistances and reduced thermal conductivities, the role of the dynamics of Cs^+ ions inside the the PbI_6 framework on thermal transport is mainly associated with phonon hardening resulting in additional channels of heat transfer. (iii) The temperature-dependent thermal conductivity in these materials can be engineered across a wide range by modifying the anharmonicity of the PbI_6 framework through hydrostatic compressions. Furthermore, inducing significant octahedral tilts can lead to more disorder scattering resulting in drastically reduced temperature dependence of thermal conductivity in $CsPbI_3$.

It is generally assumed that 'guest-host' interactions typically lead to thermal conductivity sup-

pression due to disorder scattering in crystalline solids.[12,33,52–61,79] This has mainly been attributed to 'rattling' of guest atoms inside the nanocages of the host framework and hybridization of 'guest-host' vibrational modes that lead to avoided crossings and flat bands that can span the entire vibrational spectrum. Our results, however, show that the 'guest-host' vibrational coupling in strongly anharmonic materials such as metal halide perovskites can also lead to competing effects where the 'guest' atoms can facilitate heat transfer through hardening of the vibrational modes of the 'host' framework. In other words, the dynamic motion of the A-site cations that are in phase with the vibrations of the metal halide framework can enhance heat transfer by providing additional vibrational modes to the soft framework. This marks a new mechanism of thermal transport in crystalline solids, in general, where the 'guest' species indirectly facilitate heat transfer. Our study provides the fundamental understanding of the structure-property relationship dictating thermal transport in metal halide perovskites, which will serve as a blueprint for designing these emergent class of materials that have the potential to revolutionize several applications such as photovoltaic and flexible energy harvesting devices.

IV. Methods

A. Molecular Dynamics (MD) Simulations

For our atomistic simulations, we implement our recently formulated interatomic potential capable of reproducing the temperature dependent phase transitions and accurate lattice parameters of $CsPbI_3$ as shown in Fig. S1 of the Supporting Information.[80] The potential has also been utilized to study the thermal properties of methylammoinium lead halide perovskites,[11,81,82] and has been demonstrated to reproduce several other physical attributes of metal halide perovskites such as structural and vibrational properties,[83] elastic softness,[84–86] and ionic polarization and mobilities.[87] More details regarding the interatomic potential is given in the Supporting Information.

For all our simulations, we use the large-scale atomic/molecular massively parallel simulator (LAMMPS) package.[88] Our computational domains are initially equilibrated under the Nosé-

Hoover thermostat and barostat (i.e. the NPT ensemble)[89] for 2 ns with a timestep of 0.5 fs where the number of particles, pressure and temperature of the system are held constant at 0 bar pressure. Following the NPT integration, further equilibration is carried out under the NVT ensemble where the volume and temperature are kept constant for a total of 1 ns with periodic boundary conditions in all three directions for the entire simulation. An additional equilibration is performed under NVE ensemble for 1 ns where number of particles, volume and total energy of the system are constant. Finally, we utilize the Green-Kubo (GK) formalism method to calculate the thermal conductivities of the computational domains.

For the GK formalism under the equilibrium molecular dynamics (EMD) simulations framework, the thermal conductivity of our $CsPbI_3$ structures is calculated as,

$$\kappa_\alpha = \frac{1}{k_\mathrm{B} V T^2} \int_0^\infty \langle J_\alpha(t) J_\alpha(0) \rangle dt. \tag{1}$$

where t is the time, T and V are the temperature and volume of the system, and $\langle J_\alpha(t) J_\alpha(0) \rangle$ is the αth component of the heat current autocorrelation function (HCACF) which is given as,[90]

$$\mathrm{J} = \frac{1}{V} \left(\sum_i v_i \epsilon_i + \sum_i \mathrm{S}_i \cdot v_i \right). \tag{2}$$

where, v_i, ϵ_i, and S_i represent the velocity, energy and stress of atom i, respectively. More details regarding the GK formalism is given in the Supporting Information.

B. Spectral Energy Density (SED) Calculation

We calculate the phonon properties of our inorganic halide perovskite structures from MD simulations using the SED formalism. In this technique, the atomic velocities are Fourier transformed to get the average kinetic energy per unit cell as a function of wave vector ($\boldsymbol{k}$) and frequency (ω),

which is given as,[75,76]

$$\Phi(\boldsymbol{k},\omega) = \frac{1}{4\pi\tau_0 N_T}\sum_{\alpha}^{3}\sum_{j}^{B} m_j \left| \int_0^{\tau_0} \sum_{n_{x,y,z}}^{N_T} \dot{u}_\alpha \begin{pmatrix} n_{x,y,z} \\ j \end{pmatrix}; t \Bigg) \times exp\left[i\boldsymbol{k}\cdot\boldsymbol{r}\begin{pmatrix} n_{x,y,z} \\ 0 \end{pmatrix} - i\omega t \right] dt \right|^2 . \quad (3)$$

where τ_0 is the total simulation time, N_T is the number of unit cells in the crystal, α is the cartesian direction, j is the atom label in a given unit cell, B is the atomic number in the unit cell, m_j is the mass of atom j in the unit cell, $n_{x,y,z}$ is a unit cell, $\dot{u}_\alpha \begin{pmatrix} n_{x,y,z} \\ j \end{pmatrix}; t \Bigg)$ denotes the velocity of the jth atom in the nth unit cell along the α direction at time t and $\boldsymbol{r}\begin{pmatrix} n_{x,y,z} \\ 0 \end{pmatrix}$ is the equilibrium position of each unit cell.

The phonon lifetime is calculated by manually identifying Lorentzian shaped modes and fitting each mode using the Lorentzian function which is given as,[75]

$$\Phi(\boldsymbol{k},\omega) = \frac{I}{1 + \Big[\big(\omega - \omega_c\big)/\gamma\Big]^2} \quad (4)$$

where I, ω_c and γ are the peak intensity, frequency at the peak center, and half-width at half-maximum, respectively.

For the construction of the computational domain for our SED calculations, we use a cubic $CsPbI_3$ structure with 5 atoms in the unit cell that is replicated $150 \times 2 \times 2$ to create a supercell. The longer length in the x-direction ensures a high resolution for our SED plots as shown below and in the main manuscript. Then we equilibrate the supercell structure initially under the Nose-Hoover thermostat and barostat (i.e. the NPT ensemble)[89] for 1 ns with a timestep of 0.5 fs where the number of particles, pressure and temperature of the system are held constant at 0 bar pressure. Following the NPT integration, further equilibration is carried out under the NVT ensemble where the volume and temperature are kept constant for a total of 2 ns. Finally, we performed MD simulations under the microcanonical ensemble (or NVE ensemble) for 1.5 ns using 0.5 fs timestep

and output the velocities and positions of each atoms for the SED calculation.

Supporting Information Available

The Supporting Information is available free of charge at.

Force field for $CsPbI_3$, details of the computational domain setup, equilibrium MD (EMD) simulation, vibrational density of states calculation, spectral heat flux calculation, spectral energy density calculation.

Acknowledgments

This work is supported by the Office of Naval Research, Grant No. N00014-21-1-2622. The work is also partially supported by the National Science Foundation (NSF Award No. 2119365).

References

(1) Du, M. H. Efficient Carrier Transport in Halide Perovskites: Theoretical Perspectives. *Journal of Materials Chemistry A* **2014**, *2*, 9091–9098.

(2) Veldhuis, S. A.; Boix, P. P.; Yantara, N.; Li, M.; Sum, T. C.; Mathews, N.; Mhaisalkar, S. G. Perovskite Materials for Light-Emitting Diodes and Lasers. *Advanced materials* **2016**, *28*, 6804–6834.

(3) Herz, L. M. Charge-Carrier Dynamics in Organic-Inorganic Metal Halide Perovskites. *Annu. Rev. Phys. Chem* **2016**, *67*, 65–89.

(4) Milot, R. L.; Sutton, R. J.; Eperon, G. E.; Haghighirad, A. A.; Martinez Hardigree, J.; Miranda, L.; Snaith, H. J.; Johnston, M. B.; Herz, L. M. Charge-Carrier Dynamics in 2D Hybrid Metal–Halide Perovskites. *Nano letters* **2016**, *16*, 7001–7007.

(5) Dunlap-Shohl, W. A.; Zhou, Y.; Padture, N. P.; Mitzi, D. B. Synthetic Approaches for Halide Perovskite Thin Films. *Chemical reviews* **2018**, *119*, 3193–3295.

(6) Burschka, J.; Pellet, N.; Moon, S.-J.; Humphry-Baker, R.; Gao, P.; Nazeeruddin, M. K.; Grätzel, M. Sequential Deposition as a Route to High-Performance Perovskite-Sensitized Solar Cells. *Nature* **2013**, *499*, 316–319.

(7) Williams, S. T.; Rajagopal, A.; Chueh, C.-C.; Jen, A. K.-Y. Current Challenges and Prospective Research for Upscaling Hybrid Perovskite Photovoltaics. *The journal of physical chemistry letters* **2016**, *7*, 811–819.

(8) Wei, Z.; Chen, H.; Yan, K.; Yang, S. Inkjet Printing and Instant Chemical Transformation of a $CH_3NH_3PbI_3$/Nanocarbon Electrode and Interface for Planar Perovskite Solar Cells. *Angewandte Chemie International Edition* **2014**, *53*, 13239–13243.

(9) Li, Z.; Klein, T. R.; Kim, D. H.; Yang, M.; Berry, J. J.; Van Hest, M. F.; Zhu, K. Scalable Fabrication of Perovskite Solar Cells. *Nature Reviews Materials* **2018**, *3*, 1–20.

(10) Brenner, T. M.; Egger, D. A.; Kronik, L.; Hodes, G.; Cahen, D. Hybrid Organic—Inorganic Perovskites: Low-Cost Semiconductors with Intriguing Charge-Transport Properties. *Nature Reviews Materials* **2016**, *1*, 1–16.

(11) Giri, A.; Chen, A. Z.; Mattoni, A.; Aryana, K.; Zhang, D.; Hu, X.; Lee, S.-H.; Choi, J. J.; Hopkins, P. E. Ultralow Thermal Conductivity of Two-Dimensional Metal Halide Perovskites. *Nano letters* **2020**, *20*, 3331–3337.

(12) Lee, W.; Li, H.; Wong, A. B.; Zhang, D.; Lai, M.; Yu, Y.; Kong, Q.; Lin, E.; Urban, J. J.; Grossman, J. C.; Yang, P. Ultralow Thermal Conductivity in All-Inorganic Halide Perovskites. *Proceedings of the National Academy of Sciences* **2017**, *114*, 8693–8697.

(13) Elbaz, G. A.; Ong, W.-L.; Doud, E. A.; Kim, P.; Paley, D. W.; Roy, X.; Malen, J. A. Phonon

Speed, Not Scattering, Differentiates Thermal Transport in Lead Halide Perovskites. *Nano letters* **2017**, *17*, 5734–5739.

(14) Grätzel, M. The Light and Shade of Perovskite Solar Cells. *Nature materials* **2014**, *13*, 838–842.

(15) McMeekin, D. P.; Sadoughi, G.; Rehman, W.; Eperon, G. E.; Saliba, M.; Hörantner, M. T.; Haghighirad, A.; Sakai, N.; Korte, L.; Rech, B.; Johnston, M. B.; Herz, L. M.; Snaith, H. J. A Mixed-Cation Lead Mixed-Halide Perovskite Absorber for Tandem Solar Cells. *Science* **2016**, *351*, 151–155.

(16) Chung, I.; Lee, B.; He, J.; Chang, R. P.; Kanatzidis, M. G. All-Solid-State Dye-Sensitized Solar Cells with High Efficiency. *Nature* **2012**, *485*, 486–489.

(17) Tan, Z.-K.; Moghaddam, R. S.; Lai, M. L.; Docampo, P.; Higler, R.; Deschler, F.; Price, M.; Sadhanala, A.; Pazos, L. M.; Credgington, D.; Hanusch, F.; Bein, T.; Snaith, H. J.; Friend, R. H. Bright Light-Emitting Diodes Based on Organometal Halide Perovskite. *Nature nanotechnology* **2014**, *9*, 687–692.

(18) Hong, W.-L.; Huang, Y.-C.; Chang, C.-Y.; Zhang, Z.-C.; Tsai, H.-R.; Chang, N.-Y.; Chao, Y.-C. Efficient Low-Temperature Solution-Processed Lead-Free Perovskite Infrared Light-Emitting Diodes. *Advanced Materials* **2016**, *28*, 8029–8036.

(19) Yuan, M.; Quan, L. N.; Comin, R.; Walters, G.; Sabatini, R.; Voznyy, O.; Hoogland, S.; Zhao, Y.; Beauregard, E. M.; Kanjanaboos, P.; Lu, Z.; Kim, D. H.; Sargent, E. H. Perovskite Energy Funnels for Efficient Light-Emitting Diodes. *Nature nanotechnology* **2016**, *11*, 872–877.

(20) Zhu, H.; Fu, Y.; Meng, F.; Wu, X.; Gong, Z.; Ding, Q.; Gustafsson, M. V.; Trinh, M. T.; Jin, S.; Zhu, X. Lead Halide Perovskite Nanowire Lasers with Low Lasing Thresholds and High Quality Factors. *Nature materials* **2015**, *14*, 636–642.

(21) Eaton, S. W.; Lai, M.; Gibson, N. A.; Wong, A. B.; Dou, L.; Ma, J.; Wang, L.-W.; Leone, S. R.; Yang, P. Lasing In Robust Cesium Lead Halide Perovskite Nanowires. *Proceedings of the National Academy of Sciences* **2016**, *113*, 1993–1998.

(22) Fang, Y.; Dong, Q.; Shao, Y.; Yuan, Y.; Huang, J. Highly Narrowband Perovskite Single-Crystal Photodetectors Enabled by Surface-Charge Recombination. *Nature Photonics* **2015**, *9*, 679–686.

(23) Leng, K. et al. Molecularly Thin Two-Dimensional Hybrid Perovskites with Tunable Optoelectronic Properties due to Reversible Surface Relaxation. *Nature materials* **2018**, *17*, 908–914.

(24) Haque, M. A.; Kee, S.; Villalva, D. R.; Ong, W.-L.; Baran, D. Halide Perovskites: Thermal Transport and Prospects for Thermoelectricity. *Advanced Science* **2020**, *7*, 1903389.

(25) Ferreira, A.; Létoublon, A.; Paofai, S.; Raymond, S.; Ecolivet, C.; Rufflé, B.; Cordier, S.; Katan, C.; Saidaminov, M. I.; Zhumekenov, A.; Bakr, O.; Even, J.; Bourges, P. Elastic Softness of Hybrid Lead Halide Perovskites. *Physical Review Letters* **2018**, *121*, 085502.

(26) Egger, D. A.; Bera, A.; Cahen, D.; Hodes, G.; Kirchartz, T.; Kronik, L.; Lovrincic, R.; Rappe, A. M.; Reichman, D. R.; Yaffe, O. What Remains Unexplained about the Properties of Halide Perovskites? *Advanced Materials* **2018**, *30*, 1800691.

(27) Munson, K. T.; Swartzfager, J. R.; Asbury, J. B. Lattice Anharmonicity: A Double-Edged Sword for 3D Perovskite-based Optoelectronics. *ACS Energy Letters* **2019**, *4*, 1888–1897.

(28) Batignani, G.; Fumero, G.; Srimath Kandada, A. R.; Cerullo, G.; Gandini, M.; Ferrante, C.; Petrozza, A.; Scopigno, T. Probing Femtosecond Lattice Displacement upon Photo-Carrier Generation in Lead Halide Perovskite. *Nature communications* **2018**, *9*, 1–5.

(29) Miyata, K.; Meggiolaro, D.; Trinh, M. T.; Joshi, P. P.; Mosconi, E.; Jones, S. C.; De An-

gelis, F.; Zhu, X.-Y. Large Polarons in Lead Halide Perovskites. *Science advances* **2017**, *3*, e1701217.

(30) Pisoni, A.; Jacimovic, J.; Barisic, O. S.; Spina, M.; Gaál, R.; Forró, L.; Horváth, E. Ultra-Low Thermal Conductivity in Organic–Inorganic Hybrid Perovskite $CH_3NH_3PbI_3$. *The journal of physical chemistry letters* **2014**, *5*, 2488–2492.

(31) Li, B.; Kawakita, Y.; Liu, Y.; Wang, M.; Matsuura, M.; Shibata, K.; Ohira-Kawamura, S.; Yamada, T.; Lin, S.; Nakajima, K.; Liu, S. F. Polar Rotor Scattering as Atomic-Level Origin of Low Mobility and Thermal Conductivity of Perovskite $CH_3NH_3PbI_3$. *Nature communications* **2017**, *8*, 1–9.

(32) Zhu, T.; Ertekin, E. Mixed Phononic and Non-Phononic Transport in Hybrid Lead Halide Perovskites: Glass-Crystal Duality, Dynamical Disorder, and Anharmonicity. *Energy & Environmental Science* **2019**, *12*, 216–229.

(33) Xie, H.; Hao, S.; Bao, J.; Slade, T. J.; Snyder, G. J.; Wolverton, C.; Kanatzidis, M. G. All-Inorganic Halide Perovskites as Potential Thermoelectric Materials: Dynamic Cation Off-Centering Induces Ultralow Thermal Conductivity. *Journal of the American Chemical Society* **2020**, *142*, 9553–9563.

(34) Peierls, R. Zur Kinetischen Theorie der Wärmeleitung in Kristallen. *Annalen der Physik* **1929**, *395*, 1055–1101.

(35) Srivastava, G. Phonon Conductivity of Insulators and Semiconductors. *Journal of Physics and Chemistry of Solids* **1980**, *41*, 357–368.

(36) Dove, M. T. *Introduction to Lattice Dynamics*; Cambridge university press, 1993.

(37) Hardy, R. J. Energy-Flux Operator for a Lattice. *Physical Review* **1963**, *132*, 168.

(38) Abeles, B. Lattice Thermal Conductivity of Disordered Semiconductor Alloys at High Temperatures. *Physical Review* **1963**, *131*, 1906.

(39) Cahill, D. G.; Watson, S. K.; Pohl, R. O. Lower Limit to the Thermal Conductivity of Disordered Crystals. *Physical Review B* **1992**, *46*, 6131.

(40) Garg, J.; Bonini, N.; Kozinsky, B.; Marzari, N. Role of Disorder and Anharmonicity in the Thermal Conductivity of Silicon-Germanium Alloys: A First-Principles Study. *Physical review letters* **2011**, *106*, 045901.

(41) Giri, A.; Karna, P.; Hopkins, P. E. Exceptionally Enhanced Thermal Conductivity of Aluminum Driven by Extreme Pressures: A First-Principles Study. *The Journal of Physical Chemistry Letters* **2022**, *13*, 10918–10923.

(42) McGaughey, A. J.; Jain, A.; Kim, H.-Y.; Fu, B. Phonon Properties and Thermal Conductivity from First Principles, Lattice Dynamics, and the Boltzmann Transport Equation. *Journal of Applied Physics* **2019**, *125*, 011101.

(43) Cahill, D. G.; Braun, P. V.; Chen, G.; Clarke, D. R.; Fan, S.; Goodson, K. E.; Keblinski, P.; King, W. P.; Mahan, G. D.; Majumdar, A.; Maris, H. J.; Phillpot, S. R.; Pop, E.; Shi, L. Nanoscale Thermal Transport. II. 2003–2012. *Applied physics reviews* **2014**, *1*, 011305.

(44) Cahill, D. G.; Ford, W. K.; Goodson, K. E.; Mahan, G. D.; Majumdar, A.; Maris, H. J.; Merlin, R.; Phillpot, S. R. Nanoscale Thermal Transport. *Journal of applied physics* **2003**, *93*, 793–818.

(45) Allen, P. B.; Feldman, J. L. Thermal Conductivity of Disordered Harmonic Solids. *Physical Review B* **1993**, *48*, 12581.

(46) Seyf, H. R.; Yates, L.; Bougher, T. L.; Graham, S.; Cola, B. A.; Detchprohm, T.; Ji, M.-H.; Kim, J.; Dupuis, R.; Lv, W.; Henry, A. Rethinking Phonons: The Issue of Disorder. *npj Computational Materials* **2017**, *3*, 1–8.

(47) Simoncelli, M.; Marzari, N.; Mauri, F. Unified Theory of Thermal Transport in Crystals and Glasses. *Nature Physics* **2019**, *15*, 809–813.

(48) Isaeva, L.; Barbalinardo, G.; Donadio, D.; Baroni, S. Modeling Heat Transport in Crystals and Glasses from a Unified Lattice-Dynamical Approach. *Nature communications* **2019**, *10*, 1–6.

(49) Allen, P. B.; Feldman, J. L.; Fabian, J.; Wooten, F. Diffusons, Locons and Propagons: Character of Atomie Yibrations in Amorphous Si. *Philosophical Magazine B* **1999**, *79*, 1715–1731.

(50) Ge, C.; Hu, M.; Wu, P.; Tan, Q.; Chen, Z.; Wang, Y.; Shi, J.; Feng, J. Ultralow Thermal Conductivity and Ultrahigh Thermal Expansion of Single-Crystal Organic–Inorganic Hybrid Perovskite $CH_3NH_3PbX_3$ (X= Cl, Br, I). *The Journal of Physical Chemistry C* **2018**, *122*, 15973–15978.

(51) Handa, T.; Yamada, T.; Nagai, M.; Kanemitsu, Y. Phonon, Thermal, and Thermo-Optical Properties of Halide Perovskites. *Physical Chemistry Chemical Physics* **2020**, *22*, 26069–26087.

(52) Pandey, T.; Du, M.-H.; Parker, D. S.; Lindsay, L. Origin of Ultralow Phonon Transport and Strong Anharmonicity in Lead-Free Halide Perovskites. *Materials Today Physics* **2022**, *28*, 100881.

(53) Takabatake, T.; Suekuni, K.; Nakayama, T.; Kaneshita, E. Phonon-Glass Electron-Crystal Thermoelectric Clathrates: Experiments and Theory. *Reviews of Modern Physics* **2014**, *86*, 669.

(54) Nolas, G.; Cohn, J.; Slack, G.; Schujman, S. Semiconducting Ge Clathrates: Promising Candidates for Thermoelectric Applications. *Applied Physics Letters* **1998**, *73*, 178–180.

(55) Christensen, M.; Abrahamsen, A. B.; Christensen, N. B.; Juranyi, F.; Andersen, N. H.; Lefmann, K.; Andreasson, J.; Bahl, C. R.; Iversen, B. B. Avoided Crossing of Rattler Modes in Thermoelectric Materials. *Nature materials* **2008**, *7*, 811–815.

(56) Dong, J.; Sankey, O. F.; Myles, C. W. Theoretical Study of the Lattice Thermal Conductivity in Ge Framework Semiconductors. *Physical review letters* **2001**, *86*, 2361.

(57) Wei, R.; Huiyuan, G.; Zihao, Z.; Lixia, Z. Filling-Fraction Fluctuation Leading to Glasslike Ultralow Thermal Conductivity in Caged Skutterudites. *Physical Review Letters* **2017**, *118*, 245901.

(58) Sales, B.; Mandrus, D.; Williams, R. K. Filled Skutterudite Antimonides: A New Class of Thermoelectric Materials. *Science* **1996**, *272*, 1325–1328.

(59) Meisner, G.; Morelli, D.; Hu, S.; Yang, J.; Uher, C. Structure and Lattice Thermal Conductivity of Fractionally Filled Skutterudites: Solid Solutions of Fully Filled and Unfilled End Members. *Physical Review Letters* **1998**, *80*, 3551.

(60) Mukhopadhyay, S.; Parker, D. S.; Sales, B. C.; Puretzky, A. A.; McGuire, M. A.; Lindsay, L. Two-Channel Model for Ultralow Thermal Conductivity of Crystalline Tl_3VSe_4. *Science* **2018**, *360*, 1455–1458.

(61) Lin, H.; Tan, G.; Shen, J.-N.; Hao, S.; Wu, L.-M.; Calta, N.; Malliakas, C.; Wang, S.; Uher, C.; Wolverton, C.; Kanatzidis, M. G. Concerted Rattling In $CsAg_5Te_3$ Leading To Ultralow Thermal Conductivity And High Thermoelectric Performance. *Angewandte Chemie* **2016**, *128*, 11603–11608.

(62) Bhui, A.; Ghosh, T.; Pal, K.; Singh Rana, K.; Kundu, K.; Soni, A.; Biswas, K. Intrinsically Low Thermal Conductivity in the n-type Vacancy-Ordered Double Perovskite Cs_2SnI_6: Octahedral Rotation and Anharmonic Rattling. *Chemistry of Materials* **2022**, *34*, 3301–3310.

(63) Hata, T.; Giorgi, G.; Yamashita, K. The Effects of the Organic–Inorganic Interactions on the Thermal Transport Properties of $CH_3NH_3PbI_3$. *Nano letters* **2016**, *16*, 2749–2753.

(64) Leguy, A. M.; Frost, J. M.; McMahon, A. P.; Sakai, V. G.; Kockelmann, W.; Law, C.; Li, X.;

Foglia, F.; Walsh, A.; O'regan, B. C. The Dynamics of Methylammonium Ions in Hybrid Organic–Inorganic Perovskite Solar Cells. *Nature communications* **2015**, *6*, 7124.

(65) Yue, S.-Y.; Zhang, X.; Qin, G.; Yang, J.; Hu, M. Insight into the Collective Vibrational Modes Driving Ultralow Thermal Conductivity of Perovskite Solar Cells. *Physical Review B* **2016**, *94*, 115427.

(66) Hsu, C.-S.; Wang, H.-W.; Hayashi, M. The Effects of the Lattice Modulation on the Intermolecular Motions of the MA Cations of the Tetragonal $MAPbI_3$ Phase. *Journal of the Chinese Chemical Society* **2023**,

(67) Kawano, S.; Tadano, T.; Iikubo, S. Effect of Halogen Ions on the low Thermal Conductivity of Cesium Halide Perovskite. *The Journal of Physical Chemistry C* **2021**, *125*, 91–97.

(68) Wang, Y.; Lin, R.; Zhu, P.; Zheng, Q.; Wang, Q.; Li, D.; Zhu, J. Cation Dynamics Governed Thermal Properties of Lead Halide Perovskite Nanowires. *Nano letters* **2018**, *18*, 2772–2779.

(69) Duda, J. C.; Hopkins, P. E.; Shen, Y.; Gupta, M. C. Exceptionally Low Thermal Conductivities of Films of the Fullerene Derivative PCBM. *Physical review letters* **2013**, *110*, 015902.

(70) Goodson, K. Ordering up the Minimum Thermal Conductivity of Solids. *science* **2007**, *315*, 342–343.

(71) Mukhopadhyay, S.; Lindsay, L.; Singh, D. J. Optic Phonons and Anisotropic Thermal Conductivity in Hexagonal $Ge_2Sb_2Te_5$. *Scientific reports* **2016**, *6*, 1–8.

(72) Li, Z.; Xie, H.; Hao, S.; Xia, Y.; Su, X.; Kanatzidis, M. G.; Wolverton, C.; Tang, X. Optical Phonon Dominated Heat Transport: A First-Principles Thermal Conductivity Study of $BaSnS_2$. *Physical Review B* **2021**, *104*, 245209.

(73) Carrete, J.; Li, W.; Mingo, N.; Wang, S.; Curtarolo, S. Finding Unprecedentedly Low-Thermal-Conductivity Half-Heusler Semiconductors via High-Throughput Materials Modeling. *Physical Review X* **2014**, *4*, 011019.

(74) Sootsman, J. R.; Chung, D. Y.; Kanatzidis, M. G. New and Old Concepts in Thermoelectric Materials. *Angewandte Chemie International Edition* **2009**, *48*, 8616–8639.

(75) Thomas, J. A.; Turney, J. E.; Iutzi, R. M.; Amon, C. H.; McGaughey, A. J. Predicting Phonon Dispersion Relations and Lifetimes from the Spectral Energy Density. *Physical Review B* **2010**, *81*, 081411.

(76) Thomas, J. A.; Turney, J. E.; Iutzi, R. M.; Amon, C. H.; McGaughey, A. J. Erratum: Predicting Phonon Dispersion Relations and Lifetimes from the Spectral Energy Density [Phys. Rev. B 81, 081411 (R)(2010)]. *Physical Review B* **2015**, *91*, 239905.

(77) Koza, M. M.; Johnson, M. R.; Viennois, R.; Mutka, H.; Girard, L.; Ravot, D. Breakdown of Phonon Glass Paradigm in La-and Ce-filled Fe_4Sb_{12} Skutterudites. *Nature materials* **2008**, *7*, 805–810.

(78) Mattoni, A.; Filippetti, A.; Saba, M.; Delugas, P. Methylammonium Rotational Dynamics in Lead Halide Perovskite by Classical Molecular Dynamics: The Role of Temperature. *The Journal of Physical Chemistry C* **2015**, *119*, 17421–17428.

(79) DeCoster, M. E.; Babaei, H.; Jung, S. S.; Hassan, Z. M.; Gaskins, J. T.; Giri, A.; Tiernan, E. M.; Tomko, J. A.; Baumgart, H.; Norris, P. M.; McGaughey, A. J. H.; Wilmer, C. E.; Redel, E.; Giri, G.; Hopkins, P. E. Hybridization from Guest–Host Interactions Reduces the Thermal Conductivity of Metal–Organic Frameworks. *Journal of the American Chemical Society* **2022**, *144*, 3603–3613.

(80) Giri, A.; Thakur, S.; Mattoni, A. Molecular Rotor–Rotor Heat Diffusion at the Origin of the Enhanced Thermal Conductivity of Hybrid Perovskites at High Temperatures. *Chemistry of Materials* **2022**,

(81) Wang, M.; Lin, S. Anisotropic and Ultralow Phonon Thermal Transport in Organic–Inorganic Hybrid Perovskites: Atomistic Insights into Solar Cell Thermal Management and Thermoelectric Energy Conversion Efficiency. *Advanced Functional Materials* **2016**, *26*, 5297–5306.

(82) Caddeo, C.; Melis, C.; Saba, M. I.; Filippetti, A.; Colombo, L.; Mattoni, A. Tuning the Thermal Conductivity of Methylammonium Lead Halide by the Molecular Substructure. *Physical Chemistry Chemical Physics* **2016**, *18*, 24318–24324.

(83) Mattoni, A.; Filippetti, A.; Saba, M.; Caddeo, C.; Delugas, P. Temperature Evolution of Methylammonium Trihalide Vibrations at the Atomic Scale. *The Journal of Physical Chemistry Letters* **2016**, *7*, 529–535.

(84) Caddeo, C.; Filippetti, A.; Mattoni, A. The Dominant Role of Surfaces in the Hysteretic Behavior of Hybrid Perovskites. *Nano Energy* **2020**, *67*, 104162.

(85) Mattoni, A.; Caddeo, C. Dielectric Function of Hybrid Perovskites at Finite Temperature Investigated by Classical Molecular Dynamics. *The Journal of Chemical Physics* **2020**, *152*, 104705.

(86) Rahman, M. A.; Giri, A. Uniquely Anisotropic Mechanical and Thermal Responses of Hybrid Organic–Inorganic Perovskites under Uniaxial Strain. *The Journal of Chemical Physics* **2021**, *155*, 124703.

(87) Delugas, P.; Caddeo, C.; Filippetti, A.; Mattoni, A. Thermally Activated Point Defect Diffusion in Methylammonium Lead Trihalide: Anisotropic and Ultrahigh Mobility of Iodine. *The journal of physical chemistry letters* **2016**, *7*, 2356–2361.

(88) Plimpton, S. Fast Parallel Algorithms for Short-Range Molecular Dynamics. *Journal of computational physics* **1995**, *117*, 1–19.

(89) Hoover, W. G. Canonical Dynamics: Equilibrium Phase-Space Distributions. *Physical review A* **1985**, *31*, 1695.

(90) Thompson, A. P.; Plimpton, S. J.; Mattson, W. General Formulation of Pressure and Stress Tensor for Arbitrary Many-Body Interaction Potentials under Periodic Boundary Conditions. *The Journal of chemical physics* **2009**, *131*, 154107.

TOC Graphic

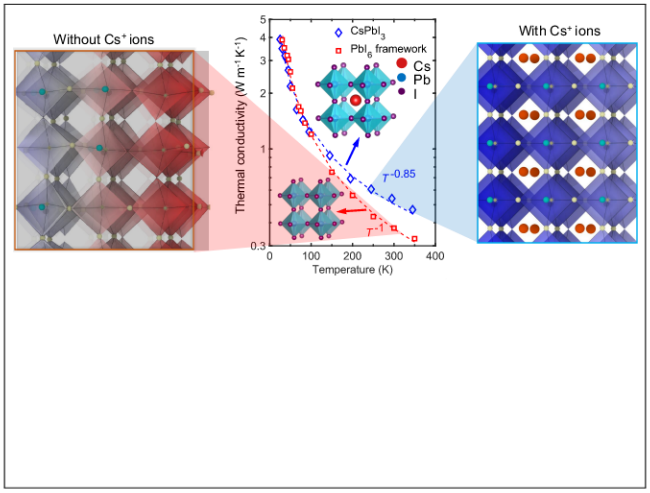
Without Cs+ ions
With Cs+ ions
CsPbI3
PbI6 framework
Cs
Pb
I
T−0.85
T−1
Thermal conductivity (W m−1 K−1)
Temperature (K)
0
100
200
300
400
0.3
1
2
3
4
5